Pure & Appl. Chem., Vol. 57, No. 10, pp. 1373–1382, 1985.
Printed in Great Britain.

Electron microscopy and diffraction of modulated structures

J.Van Landuyt, G.Van Tendeloo and S.Amelinckx*

University of Antwerp, RUCA
Faculty of Sciences, Groenenborgerlaan 171, B-2020 Antwerpen, Belgium

ABSTRACT

It is the purpose of this review to illustrate the possibilities of electron microscopy and electron diffraction techniques for the study of modulated structures. A classification of these structures according to the type of modulating structural deviation is proposed. Some particular procedures are outlined for electron diffraction as well as transmission electron microscopy observations. Also the use of the structure imaging mode is discussed since it provides detailed information on the modulation type.
Two particular examples are treated in some more detail since each illustrates particular applications of the above mentioned techniques: the charge density wave related phases in tantalum disulphide and an incommensurate intermediate phase near the α-β- transition in quartz.

INTRODUCTION

The interest expressed by various fields of materials research in the application of electron microscopy and electron diffraction for the acquisition of detailed structure data largely proves its utility for the characterization of solids. Successively physicists, metallurgists structural chemists, ceramists and mineralogists have shown growing interest in this technique by which a wealth of information can be obtained from the combined use of the electron optical possibilities of a modern electron microscope. It is the purpose of this review to illustrate in particular the applications to the characterization of modulated structures.

Modulated structures can be of various origins and in many cases they can be consider as resulting from the more or less periodic occurrence of a structural feature. A classification based on the type of interfaces and their identification criteria will be outlined. The observation techniques available in an electron microscope will be discussed with respect to their usefulness for the analysis of modulated structures.

Two case studies of modulated structures will be treated in some detail : the charge density wave driven transitions and phases observed in tantalum disulphide and incommensurate modulated structures near the phase transition $\alpha \rightarrow \beta$ in quartz.

MODULATED STRUCTURES - INCOMMENSURATE STRUCTURES

Much attention was paid lately to modulated structures and incommensurate structures. Since these concepts are part of the subject of this paper it may be useful to remind their definitions.

A structure which can be considered as resulting from a simpler basic structure by the periodic introduction of a structural feature that modifies this basic structure is called a **modulated structure**; it thus consists of periodically modified **modules** of basic structure. The structural feature may be a periodic relative shift along a planar interface, a periodic deformation pattern or a periodic composition variation, giving rise to three classes of modulated structures (Table 1). The distinction between these classes is not rigorous: any composition modulated structure is presumably also somewhat deformation modulated with the same period whereas any interface modulated structure is to some extent deformation modulated as well since often relaxation occurs along the interfaces; it may moreover also be composition modulated.

(*) Also at SCK/CEN, Mol

The table classifies modulated structures following the various types of structural deviations which can be:

- a planar defect such as a stacking fault, an antiphase boundary, a twin boundary, an inversion boundary
- a deformation of the structure caused by a spatially periodic physical phenomenon such as a charge density wave
- a periodic composition fluctuation.

The defect can have a **conservative** character whereby the composition at the defect is the same as that throughout the structure, but it can also be **non-conservative** whereby its periodic occurrence results in a measurable composition change exemplified in crystallographic shear structures and some alloy microtextures.

If the periodicity of the recurrent structure deviation is not rationally related with that of the basic structure the modulated structure is called **incommensurate**. Its diffraction pattern will then reveal satellite reflections at distances from the basic spots which also are not rationally related with the distance between these basic spots.

A short list of examples of each are mentioned in the last column of the table.

Various types of modulated structures are found : **polytypes**, occurring in some ceramics and alloys, **long period antiphase boundary structures** (LPAPB) in alloys, **crystallographic shear structures** (CSS) as known to occur in nonstoichiometric oxides; **charge density wave structures** as revealed by periodic lattice distortions (CDW).
Composition modulated structures (CMS) are sometimes revealed by the periodic repetition of structural units with a different composition; the composition can also vary continuously.

TABLE 1. Modulated structures

Modulation type	Structural deviation	Resulting structure type	Example
INTERFACE	Stacking fault	Polytypes	SiC
	Antiphase boundary	Long period APB structure 1 or 2 dimensional	Alloys
	Crystallographic shear plane	Shear structures	TiO_{2-x}
	Inversion boundary	Long period IB-structure	γ-brass
	Twin boundaries	Twin modulated structures	SiO_2
DEFORMATION	Charge density wave	Deformation M.S.	TaS_2
COMPOSITION	Structure units	Mixed layer compound	Ba-ferr.
	Composition wave	Chimney ladder	Mn-Si
	Vacancy order in planes		$Cu_{2-x}S$

Since the periods involved are of the magnitude of a few lattice spacings of the basic structures two types of observation are particularly useful for the characterization of these structures : diffraction techniques and high resolution electron microscopy.

TECHNIQUES OF OBSERVATION

a) Electron diffraction

The main advantages of using electron diffraction for the study of modulated structures stem from the large atomic scattering factor for electrons ($f_e \sim 10^4 f_x$) which enables:

1° smaller quantities of material to be analysed and smaller effects to be detected
2° sensitive registration in the case of dynamic phenomena.

Let us first illustrate the effect of a crystal containing a **periodic lattice distortion** on the geometrical aspects of a diffraction pattern (ref.1). The positions of the diffraction spots in the kinematical approximation for a structure deformed by small periodic distortions characterized by a Fourier expansion of which $w_{\bar{H},\bar{G}}$ are the coefficients, are given by the maxima of the diffraction amplitude :

$$A(\bar{g}) = \sum_{\bar{H}} v_{\bar{H}}\, \delta(\bar{g} - \bar{H}) - i \sum_{\bar{H}} \sum_{\bar{G}} v_{\bar{H}} w_{\bar{H},\bar{G}}\, \delta[\bar{g} - (\bar{H}+\bar{G})]$$

Here $\bar{g}$ is the position vector in reciprocal space $v_{\bar{H}}$ the fourier coefficient of the lattice potential, $\bar{H}$ the reciprocal lattice vector for the undistorted crystal. This

expression shows that the diffracted intensity will have maxima determined by the δ-functions at positions :

$$\bar{g} = \bar{H} \quad \text{and} \quad \bar{g} = \bar{H} + \bar{G}$$

i.e. at the reciprocal lattice nodes of the basic lattice (which remains unchanged by the periodic distortion), and at points which can be derived from these reciprocal points by adding vectors $\bar{G}$, which are the reciprocal lattice vectors of the distortion pattern.

The $w_{\bar{H},\bar{G}}$ decrease rapidly for the higher harmonics at least for quasi-harmonic distortion waves, only two or at most three terms have therefore to be considered; as a consequence also the coefficients $v_{\bar{H}}$, $w_{\bar{H},\bar{H}.\bar{G}}$ will be small compared to the coefficients $v_{\bar{H}}$ which means that these "satellite" reflections will be weak as compared to the basic reflections.
The coefficients $w_{\bar{H},\bar{G}}$ are of the form $w_{\bar{H},\bar{G}} = 2\pi(\bar{H}.\bar{A})$ with $\bar{A} = A\bar{e}_u$, where A is the amplitude of the wave with wave vector $\bar{G}$ and where $\bar{e}_u$ characterizes the polarization of the deformation wave. In diffraction one only detects the projection of $\bar{A}$ on $\bar{H}$. It is further clear that the magnitude of $w_{\bar{H},\bar{G}}$ increases linearly with the length of $\bar{H}$. The intensity of the spot at $\bar{H}+\bar{G}$, which is proportional to $|v_{\bar{H}}|^2|w_{\bar{H},\bar{G}}|^2$ will therefore be a function of the intensity of the matrix spot at $\bar{H}$ (itself proportional to $|v_{\bar{H}}|^2$) which becomes relatively larger for larger $\bar{H}$ values. This provides us with a means of distinguishing a deformation modulated structure from a regular superstructure. This trend is observed in the diffraction patterns of **periodically distorted structures** observed in TaS_2 which will be discussed in the next chapter.

We now discuss the effect of **periodic sequences of planar translation interfaces** on the diffraction pattern. It will be shown how the positions of the resulting satellite reflections can be used to determine the displacement vector of the planar defects, their orientation and their spacing. Together with the direct space evidence from the image this will enable all characteristics of the interface modulated structure to be derived.

Using the kinematical approximation, which is sufficient if one is interested only in the spot positions, it can easily be shown that satellites occur at positions $\bar{g}$, shifted with respect to the basic reflection $\bar{H}$, and given by (ref.2).

$$\bar{g} = \bar{H} + \frac{1}{d}(m - \bar{H}.\bar{R})\bar{n}$$

Here $\bar{n}$ is a unit vector perpendicular to the translation interfaces, $\bar{R}$ their displacement vector and d their spacing, m is an integer (i.e. the order of the satellite).
The physical situation, which is in particular applicable to the study of crystallographic shear structures and long period antiphase boundary structures, is illustrated in figure 1.

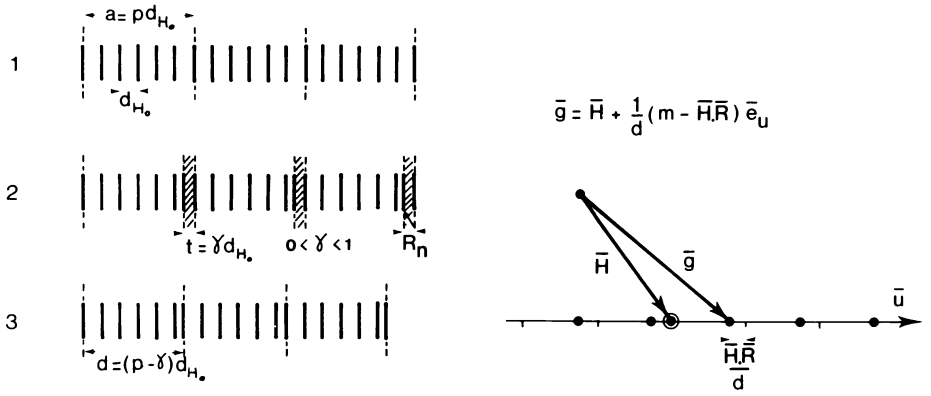

Fig.1.Satellite characteristics for periodic planar defects.

1. At regular intervals $a = pd_{H_o}$ with respect to the basic spacing d_H.
2. Defects are introduced characterized by a displacement vector $\bar{R}$.
3. The resulting superstructure has a period $(p-\gamma)d_{H_o}$.

   The diffraction configuration is depicted to be right.

It is clear that the measurement of the fractional shifts of the rows of satellites with respect to the basic reflections for three independent reflections $\bar{H}$ is sufficient for the determination of the displacement vector $\bar{R}$.

The method is easily extended to two-dimensional interface modulated structures and can use-

fully be applied to block structures and 2D LPAPB structures in alloys (ref.3). It was also extended and applied to periodic twin configurations (ref.4).

As mentioned in the introduction, the large scattering factor enables dynamic changes to be recorded in diffraction but also the selection of very small areas by the selected area diffraction technique.
This technique of selection which in a conventional electron microscope is practically limited to about 1 μm can be extended nowadays by beam-selecting methods down to a few nanometer units of crystal area. This range can also be reached by **optical diffraction methods** applied to high resolution negatives. In the latter method the microscope negative is used as a diffraction grating for a laser diffractometer whereby a physical aperture of a few millimeters enables areas as small as a few nanometers to be selected and diffraction effects registered. Using these diffraction effects microtextures, orientation variants and even single defects can be analysed (ref.5).

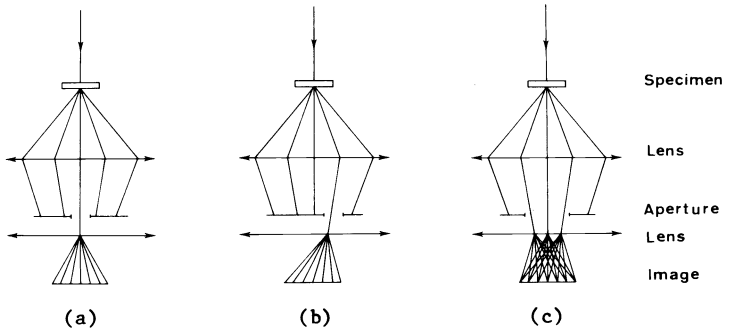

Fig.2.Imaging modes in transmission electron microscopy.
(a) Bright field imaging
(b) Dark field imaging
(c) Multiple beam imaging

b) Electron microscopy images - Direct space evidence

Valuable information on modulated structures can also be obtained from transmission images in electron microscopy.
Two observation modes have to be considered : 1. Diffraction contrast images at low magnification and 2. High magnification high resolution images.

1. Diffraction contrast images - low magnification.

The elastic interaction of high energy electrons with crystalline materials is very sensitive to local changes in crystalline periodicity and orientation. There are three modes of observation which are often used in transmission electron microscopy studies. (fig.2). The bright field mode (a) whereby only the direct beam is used for imaging and the dark field mode (b) whereby a single strongly diffracted beam is allowed in the imaging lens system will be discussed first. Images obtained using these modes rely for their interpretation mainly on the two-beam electron diffraction theory which enables the interpretation of structure defects by well understood and reliable procedures (ref.6).

It is intuitively clear that structure factor changes and local orientation differences, will influence the diffraction intensities and consequently the transmission image which is an enlarged mapping of the beam intensity at the exit face of the crystal foil. As a consequence crystalline phases differentiated by differences in structure factor, give rise to differences in background intensity. It allows one to observe directly phase changes or transformation fronts between phases and their evolution upon exterior influences such as heating, cooling, straining, etc.

By using the dark field technique whereby a spot originating from only one of the phases is selected for imaging, only the area which is in this phase state will light up, and the interphase boundary will very clearly be observed. This effect will be illustrated in the movie on TaS_2; an example of a phase front evolution is shown in fig.9.

As a result of the sensitivity of electron diffraction for local orientation differences, grain boundaries, twins, ordering domains (variants) become observable as well as defects such as dislocation lines and defect clusters by the strain field which they produce.

For Figs. 3,5,7 & 9 see PLATE I (facing p.1376) • For Figs. 10,12,13 & 14 see PLATE II (facing p.1377)

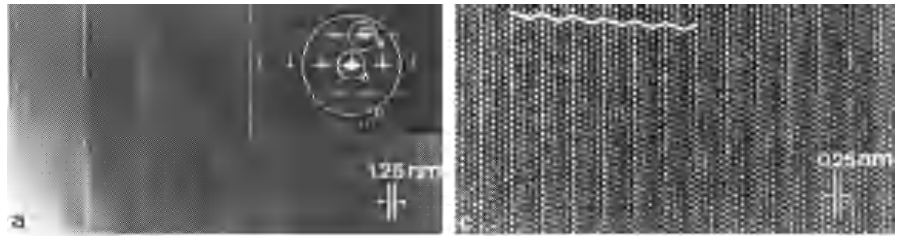

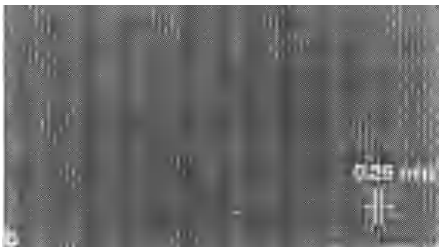

Fig. 3

High resolution electron micrographs of the 15R-SiC structure obtained under different experimental conditions.
(a) Using a small objective diaphragm (see A in inset).
(b) Using a larger objective aperture (including the 00.15 reflection); only the central row is excited.
(c) Using a large objective diaphragm (see C in the inset).
In the [11$\bar{2}$0] orientation an image directly related to the projected crystal structure can be obtained.

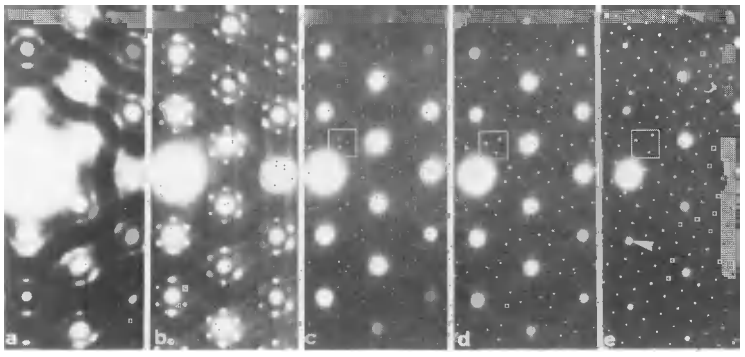

Fig. 5

Sequence of diffraction patterns corresponding with the various intrapolytypic phase transitions in 1T-tantalum disulfide as observed upon cooling from 570 K. Patterns (b) (c) and (d) are incommensurate, pattern (d) is due to the commensurate low temperature superstructure phase.

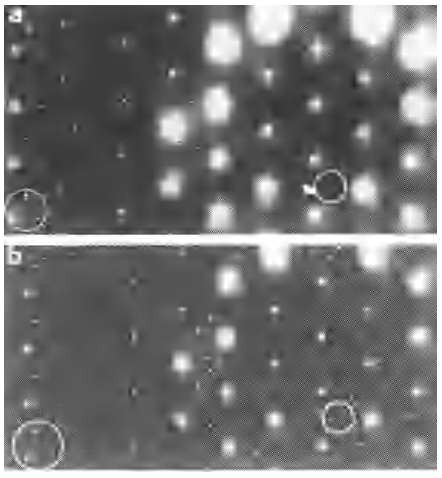

Fig. 7

(a) Electron diffraction pattern of the $1T_\beta$-phase. Notice the small triangles of spots in the center of the triangle of basic spots and nearly equilateral to it. The camera length for figs. 7a and 7b was chosen in such a way that at the edge of the pattern the higher level of the octahedral complex is visible.

(b) Diffraction pattern of the $1T_\gamma$-phase. The small triangle has changed orientation and has become larger.

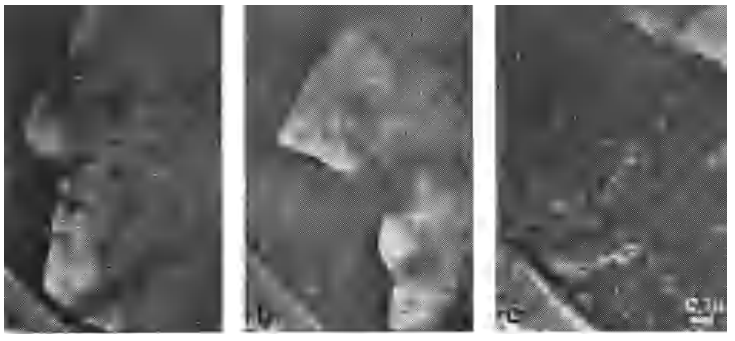

Fig. 9

Diffraction contrast image of the phase front between the $1T_\gamma$-and $1T_\beta$-phase. Dark field images in a $1T_\gamma$-reflection reveal this phase as bright areas. Successive stages of the phase front are shown.

P L A T E I

page facing p.1376

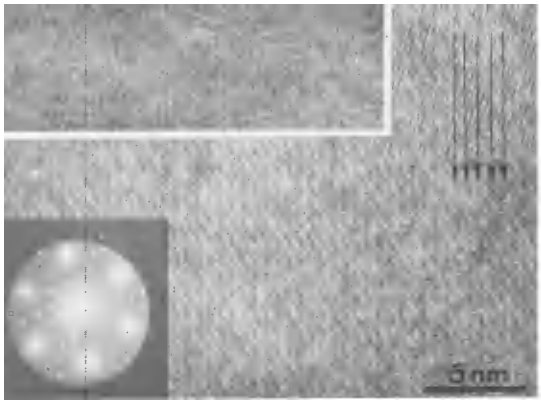

Fig. 10

Bright field lattice image of the room temperature incommensurate phase of TaS_2. The beams used to make the image are those shown in the inset. The directions of the deformation waves and of the close-packed atom rows are indicated; they enclose an angle of about $18° + 1°$. A look at grazing incidence along the indicated direction is photographed in the top part; it allows to observe the deformation waves more clearly.

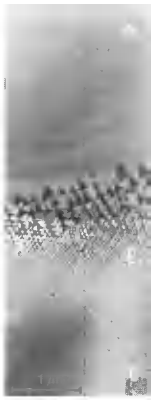

Fig. 12

A gradient from top to bottom of this quartz crystal area across the transition temperature. A dense network of Dauphiné twins is observed to constitute an intermediate incommensurate superstructure.

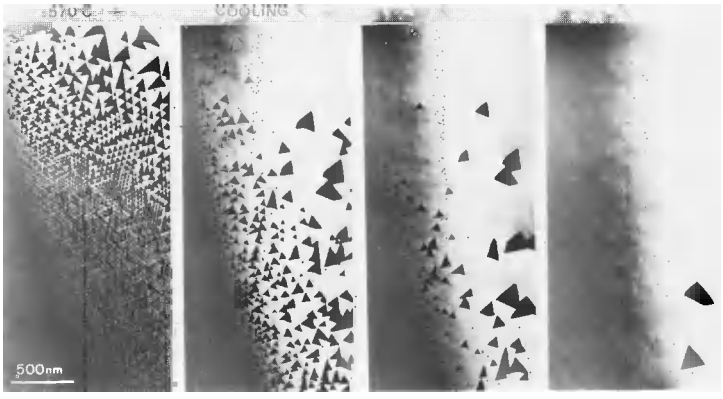

Fig. 13

Successive stages of a cooling cycle from close to the transition at 573°C to room temperature on the same crystal region. Close to the transition temperature a regular hexagonal network of Dauphiné twin domains is formed. They are revealed by the black- white structure factor contrast.

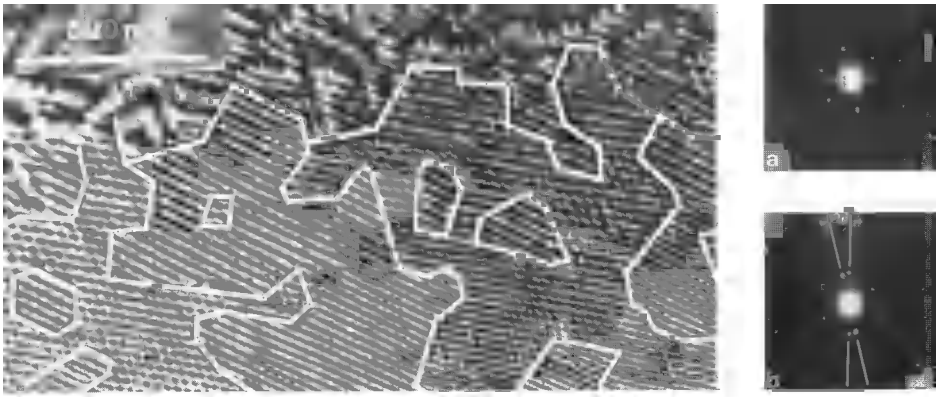

Fig. 14

Quartz crystal observed in a temperature gradient where macrodomains in the intermediate phase near the α-β transition are clearly observed. The change in q-vector orientation between the macrodomains increases with ΔT from the transition which is situated past the bottom of the figure. The insets are optical diffraction patterns of a) single macrodomain and b) across the boundary of two macrodomains.

PLATE II

page facing p.1377

2. Structure imaging mode.

As illustrated in fig.2 (c) many diffracted beams can be allowed to interfere and enter in the magnifying lens system. Modern electron microscopes in which lens defects and electronic and mechanical stability have been improved, allow for the higher angle beams to contribute in a non detrimental way to high magnification images. This multibeam-mode is then called **high resolution structure imaging**; if certain precautions are taken concerning specimen thickness, precise alignment along a zone-axis, controlled focusing conditions etc., resolution figures for structure imaging of 0.25 nm can be reached.

This mode is very useful for the analysis of modulated structures since it enables to visualize the structure nearly down to the atomic scale; in particular it allows to determine the origin of the modulation. However it should be born in mind however that the interpretation down to this scale **should** be complemented by structure image calculations. A review of these calculation methods was given by Spence (ref.7) and recent advances with respect to multislice algorithms were reported by Coene and Van Dyck (ref.8,9).
An illustrative example of the possibilities of the technique is shown in fig.3 a,b,c where various imaging modes producing increasing detail were used for characterizing the 15R polytype of SiC (ref.10).

The information to be expected from the lattice imaging technique largely depends on the resolving power of the microscope and on the size and position of the objective aperture. The 15R polytype which has a stacking sequence |AB CBA|CA BAC|BC ACB|...consists of three blocks of five layers which are equivalent but shifted over one third of a lattice vector. The repeat unit perpendicular to the layers will be 5 x 0.251 nm = 1.255 nm thick.

When selecting the central beam and two or three reflections on both sides (circle indicated A in inset) information can be expected about the long period. The 1.255 nm fringe period is revealed (fig.3 a) and for a number of years this imaging mode has been succesfully applied to identify different polytypes. Defects in the stacking sequences (stacking faults) are revealed as a local variation in the spacing (see fig.3 a) or as a variation in fringe intensity. Similar images are obtained in the dark field imaging mode when a similar size objective aperture is positioned as shown e.g. in B of the inset. These dark field images have the further advantage that in the case that twinning is present along the layer planes, the twinned parts are revealed as bands of uniform contrast superposed on the line images (ref.11).

With a more recent electron microscope it makes sense to use a larger aperture, including for instance the fundamental (00.15) reflections on both sides of the central beam. If non-central rows are excluded (mode A) the 0.251 nm spacing of the individual SiC layers is revealed (fig.3 b) i.e. detailed subunit cell information in one direction becomes available. Under suitable diffraction conditions however (e.g. when viewing along $[11\bar{2}0]$) and including also non-central row reflections in the objective aperture (mode C in inset) the high resolution image will provide detailed information about the stacking sequence. An image of the 15R polytype was obtained in a 200 kV EM with 0.25 nm resolution (fig.3c).

RESEARCH EXAMPLES

A. Modulated structures in TaS_2

Tantalum disulphide undergoes various phase transitions leading to modulated structures, it is therefore a very illustrative example for demonstrating the possibilities of electron microscopy and electron diffraction. (refs.12,13,14).
Charge density wave driven periodic deformation waves give rise to a number of modulated structures within the 1T-polytype of TaS_2 (**intrapolytypic** transitions). At higher temperatures shear processes result in the transformation into other polytypes (**interpolytypic**) which are examples of interface modulated structures.

Table 2 summarizes the transitions and gives a nomenclature for the phases occurring in TaS_2.

TABLE 2

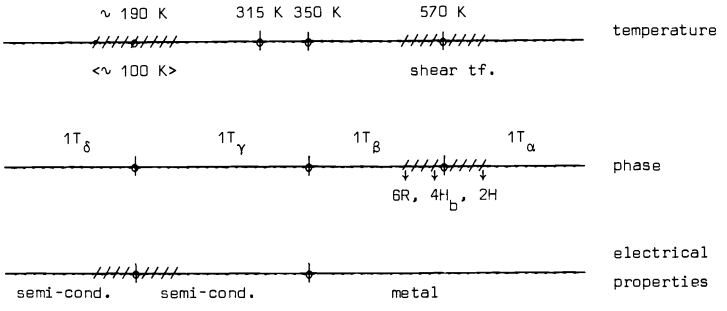

For Figs. 3,5,7 & 9 see PLATE I (facing p.1376) • For Figs. 10,12,13 & 14 see PLATE II (facing p.1377)

At high temperature (i.e. above ± 900 K) tantalum disulphide crystallizes in the simple $Cd(OH)_2$ structure with octahedral coordination. This modification can easily be retained at room temperature by moderately fast cooling and is called the 1T-phase. Its layer structure can be represented by the stacking symbol ...aγb aγb ...

Around 570 K this phase transforms by a shear mechanism into the 2H-form which is the stable room temperature phase with a structure containing trigonal prismatic layers...aβa cβc ...
Other polytypes such as 6R and $4H_b$ form at intermediate temperatures with a stacking containing octahedral as well as prismatic layers.

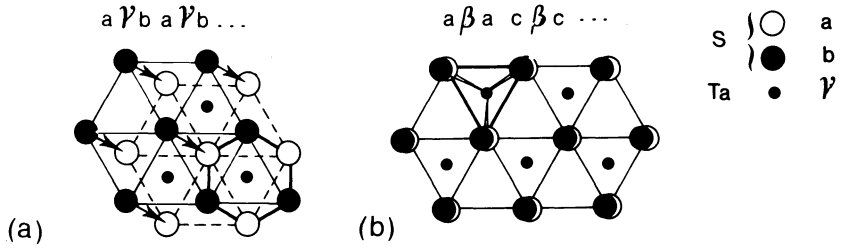

Fig.4.Structure model projected along the c-axis for the 1T (a) and 2H (b) phases of TaS_2. In the 1T-phase the cations appear in octahedral coordination whereas in the 2H-phase the coordination is trigonal prismatic.

At temperatures below 570 K the 1T form undergoes a number of **intrapolytypic** phase transitions as shown in table 2 and we shall now discuss the diffraction aspects associated with these transitions.

A.1. Distortion modulated structures

a) diffraction effects

Since TaS_2 is a layer structure, specimens for TEM are easily prepared by cleavage along the c-layers. As a consequence the electron beam is mostly oriented along the c-axis and gives rise in diffraction to a basic pattern consisting of a perfect hexagonal array of main reflections as is evident in figure 5.

Let us now briefly discuss the diffraction patterns as observed on the same crystal region and as a function of decreasing temperature.
Close to 570K one observes the pattern of fig. 5a. Apart from the main spots which are due to the basic structure, one notes incommensurate satellites around the main spots as well as curves of diffuse scattering passing through these satellite spots. The diffuse scattering can be attributed to a Kohn anomaly and information concerning the geometry of the Fermi surface can be obtained from the diffuse scattering.
These satellites are situated in planes at ± 1/3c* and form an octahedral complex of points in reciprocal space. Apart from using tilting experiments the curvature of Ewald's sphere can also quite readily be used to arrive at this conclusion which is summarized in fig.6. The spots labelled ℓ = o are in the basal section of reciprocal space.

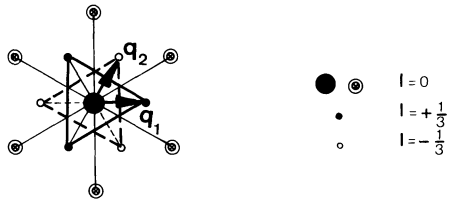

Fig.6.Configuration of satellites around each basic spot. The arrows represent the q-vectors of the deformation waves.

Upon further cooling the diffuse scattering concentrates more and more into the octahedral complex which then decreases in intensity as compared to that of small triangular arrangements of weak spots appearing in the center of the triangle of basic spots (fig.5c). This pattern is typical for the $1T_\beta$-phase.

An observation such as fig.7a, where a small camera length is used clearly illustrates the geometry of the intensity maxima. Due to the curvature of Ewald's sphere the part to the right of the pattern only reveals the o-level spots i.e. basal spots plus the small triangles; in the part to the left where Ewald's sphere rises above o-level a triangle is observed constituting the top three spots of the octahedral complex; this clearly confirms the model of fig.6 for the reciprocal space geometry.

For Figs. 3,5,7 & 9 see PLATE I (facing p.1376)● For Figs. 10,12,13 & 14 see PLATE II (facing p.1377)

At 350 K the pattern suddenly changes reversibly into that shown in figs.5d and 7b, i.e. the octahedral complex suddenly changes its orientation, producing now a larger triangular arrangement of spots in the center of the triangles of main spots. This pattern is characteristic of the $1T_\gamma$-phase. The pattern of fig.5c as well as that of fig.5d present spacing and orientation anomalies; they are clearly incommensurate. The orientation relation between these patterns and their relation to the octahedral complex is clearly illustrated in figs.8a and 8b, where the configuration of large triangles is shown to result from an 11° rotation with respect to the $1T_\beta$ orientation of the octahedral complex.

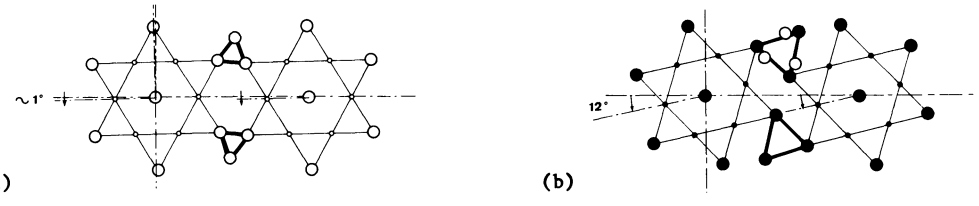

Fig.8. Illustration of the rotation of the octahedral complex explaining the origin of the small triangles of spots, their size and orientation.

The discontinuous rotation of the octahedral complex can be clearly observed at the left edge of figs.7a and 7b. The triangles of spots enclosed in the larger circle are at a level of ~ (1/3)c*: the three upper spots of the octahedral complex are observed in two discrete positions differing 11° in orientation. The vectors joining the basic reflections (invisible in this region of reciprocal space because of E.S. curvature) with these spots can be considered as the q-vectors corresponding with the periodic lattice distortions associated with the charge density waves.

On cooling the specimens below room temperature the pattern of superlattice spots (satellite) of fig.5d gradually changes in orientation with respect to the pattern of basic spots until finally the whole pattern becomes commensurate around 190K. This pattern is typical of the $1T_\delta$-phase (fig.5e). The crystal has now acquired a commensurate superstructure for which the base vectors of the reciprocal lattice are related with those of the basic structure ($\bar{A}1$) and $\bar{A}_2$) by :

$$13\ \bar{A}_1^S = 3\bar{A}_1 + \bar{A}_2$$
$$13\ \bar{A}_2^S = 4\bar{A}_1 - 3\bar{A}_2$$

b) diffraction contrast images

A very important advantage of electron microscopy techniques is the combined use of reciprocal space (diffraction) and direct space information (image). The diffraction data provide us with lattice parameters and q-vectors but the images can also yield important information on the spatial origin of particular reflections, on the presence of phases, their configuration, on the existence of domains, orientation variants etc.

The dark field imaging technique, whereby a single reflection is allowed to enter the magnifying lens system often yields interesting information. Indeed, only that area will appear bright which has caused this particular reflection. By allowing, with a very small aperture in the back focal plane of the objective lens, only a type γ-reflection (large triangle) to contribute to the image, the corresponding phase $1T_\gamma$-phase will appear bright.
Figs.9a, b and c were taken under these conditions from the same area only seconds apart in time and with the specimen at the transition temperature. A transformation front is observed at the line separating dark and light regions. On the figure different positions of such an interphase boundary are observed; it can easily be moved by the slight temperature changes caused by the heating effect of the electron beam. Whereas in (a) nearly the whole region is in the low temperature phase (imaged bright in type γ-spot) in (b) and (c) the crystal is partly transformed to a different extent. The transformation is reversible and the phase front can be moved back and forth by focussing and defocussing or by shifting the electron beam.

c) high resolution images

Another mode of operation enables the direct imaging of the deformation waves resulting from the CDW i.e. by allowing basic spots together with their satellites to contribute to a high resolution image along the [0001] zone axis. If an electron microscope with the appropriate resolving power is used the periodic lattice distortions will be directly observed, and one could expect to find evidence for the 13-point Ta-atom clusters as suggested by C.J.Van Bruggen et al (ref.15).

For Figs. 3,5,7 & 9 see PLATE I (facing p.1376) • For Figs. 10,12,13 & 14 see PLATE II (facing p.1377)

Such an image is shown in figure 10 where the inset illustrates the $1T_\gamma$-phase. The geometry of the pattern of white dots is consistent with the assumption that these dots represent tantalum atoms, which form columns along the zone axis in the undeformed structure. The atom displacements due to the presence of charge density waves are presumably too small to be detected unambiguously as displacements of individual bright dots. Moreover the rhombohedral stacking of clusters will disturb somewhat the column structure and broaden the projected Ta positions. Nevertheless when looking at grazing incidence along the indicated directions as illustrated in the top part of figure 10 somewhat darker lines can be observed.
The wave vectors of the deformation waves, as deduced from the electron diffraction pattern along the c-zone are directly related with the observed spacing and direction of the lines. The directions and the spacing of the dark lines are also consistent with the projected tantalum concentration waves (ref.16).

A.2. Interface modulated structures : polytypes

Heating the 1T-TaS_2 samples at 570 K transforms the crystal into the 2H-phase which is a polytype structure of the 1T-phase; it can be described as the 1T-phase modulated by periodic stacking faults (ref.14,b).

Although the preferred cleavage plane (0001) of this material is unfavourable for the direct observation of these faults which ly in planes perpendicular to the observation direction, the analysis of the shear dislocation images for orientation and burgers vectors and the direct observation of very intense dislocation movement allowed us to propose the following transformation mechanism based on the passage of Shockley partial dislocations between the appropriate (every two) layers. The shear transformation process is illustrated in table 3. The stacking symbols for layers are those of figure 4. The vertical lines indicate the passage of a partial dislocation changing the symbols to their right into the symbols obtained by cyclic permutation.

TABLE 3. The 1T to 2H shear transition in TaS_2

a | γb	aγ | b		aγb	aγb	aγb ...
(1) | βa	cβ | a		cβa	cβa	cβa ...
	(2) | c		bαc	bαc	bαc ...
		(3)	aγb	aγb	aγb ...
... aβa	cβc		aγb	aγb	aγb ...
2H			1T		

Also other polytypes such as $4H_b$ can be generated in a similar way and were observed in this study.

B. Quartz : an incommensurate superstructure close to the α→β phase transition

Quartz is well known to undergo a phase transition at 573C from the low quartz α-phase to the high quartz β-phase. α-quartz is rhombohedral and belongs to the pointgroup 32 whereas β-quartz is hexagonal and belongs to pointgroup 62. The loss in symmetry is clear from the projection along the c-axis in figs.11(a) to (c). Both the α and the β structures are represented and the α phase is represented in its two variants, α_1 and α_2. The structure consists of interlinked SiO_4 tetrahedra which are projected as trapezia in the α phase and as squares in the β-phase. The relationship between the α_1 and the α_2 variants is that of a 180° rotation twin with the c-axis as twin axis: the Dauphiné twin relationship.

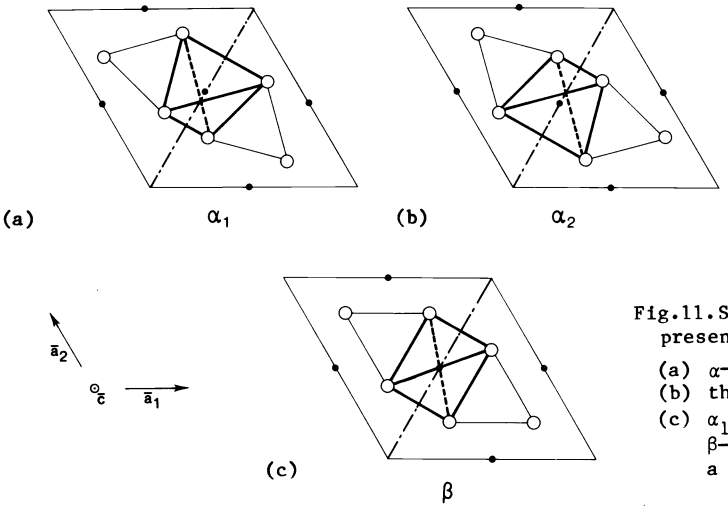

Fig.11. Structure model for quartz as presented along the c-axis.
(a) α-quartz, one variant e.g. α_1,
(b) the other variant of α-quartz, α_2,
(c) α_1, α_2 and the projection of the β-phase (tetrahedron projected as a square).

For Figs. 3,5,7 & 9 see PLATE I (facing p.1376) • For Figs. 10,12,13 & 14 see PLATE II (facing p.1377)

Although this transition has often been studied and by many different techniques, a detailed microstructural interpretation of the actual physical processes involved was not yet available (ref.17). It was therefore hoped that electron microscopy could shed some light on the process by direct observation. Ion beam thinned specimens were heated in the heating specimen holder and a temperature gradient was produced by local heating with the electron beam.

Close to the transition a large number of defects is observed. These defects are very mobile at temperatures just below the transition. In bright field images these defects are hardly visible, whereas a pronounced dark-light contrast is observed in the dark field images of particular reflections such as e.g. the $(30\bar{3}1)$ reflection in fig.11. The contrast features together with the observation of only two variants allow us to identify these defects as the Dauphiné twins described above, and the contrast as structure factor contrast.

Indeed the extinction distances (structure factors) for some reflections which are simultaneously excited in the two crystal parts are drastically different e.g. for $30\bar{3}1$ $t_{\alpha 1}$ = 605 nm, $t_{\alpha 2}$ = 144 nm. In fig.12 a typical configuration of defects is shown: a temperature gradient of a few degrees across the observed region is produced by the electron beam The closer to the transition the smaller the mesh size of the regular network of domains becomes until it reaches sizes below the resolution limit of the microscope which is about 5 nm under these experimental condition. (situation at the bottom of figure 12).

Upon cooling, as the sequence of photographs in figure 13 shows, the mesh size increases and one of the α-variants disappears at the expense of the other. Eventually some single Dauphiné twin domains remain at room temperature.

These periodic arrays of Dauphiné twin columnar domains can be considered as an incommensurate superstructure of the quartz structure.

Recently the existence of this incommensurate phase has been confirmed by other techniques such as neutron diffraction (ref.18), X-ray topography and micro Laue-techniques(ref.19). Both these studies confirm the idea of an incommensurate phase with a varying q-vector with a length in the range of 10-15 nm which in the electron microscopy observations can directly be read off from the images. Our observations inspired theoretical considerations of Aslanyan and Levanyuk (ref.20) based on Landau theory from which an incommensurate phase of dauphiné domains could be predicted. These authors conjectured the occurrence of two possible q-vectors enclosing an angle of 10-20°. Based on their theory Walker predicted the possible domain wall configurations (ref.21). He also suggested the existence of macrodomains of periodic Dauphiné twin arrays of the two above mentioned orientations for the $\bar{q}$-vectors. Figure 14 clearly proves the existence of these macrodomains and the angular difference as a function of ΔT from the transition temperature is clearly observed (ref.22).

Optical diffraction of the TEM negatives as in fig.14 can be used to analyse the q-vector orientation difference. The inset (a) illustrates an O.D. pattern of a single domain of periodic Dauphiné twins whereas the pattern marked (b) was made by selecting across the boundary of two macrodomains. The reflections reveal the q-vectors of the incommensurate phase, and the angular difference between two macrodomains is clearly evident from the splitting 2ε in inset (b).

REFERENCES

1. J.Van Landuyt, G.Van Tendeloo and S.Amelinckx, Phys.Stat.Sol.(a), 26, K9 (1974).
2. J.Van Landuyt, R.De Ridder, R.Gevers and S.Amelinckx, Mat.Res.Bull.,5, 353 (1970).
3. G.Van Tendeloo, R.Wolf, J.Van Landuyt and S.Amelinckx, Phys.Stat.Sol.(a), 47, 539 (1978).
4. D.van Dyck, D.Colaïtis and S.Amelinckx, Phys.Stat.Sol.(a), 68, 385 (1981).
5. G.Van Tendeloo and J.Van Landuyt, J.Microsc.Spectrosc.Electr., 8, 461 (1983).
6. S.Amelinckx and J.Van Landuyt, Diffraction and Imaging Techniques in Material Science, p.105, North-Holland, Amsterdam (1978).
7. J.Ch.Spence, Experimental High Resolution Electron Microscopy, Clarendon, Oxford (1981).
8. D.Van Dyck, J.Microsc., 132, 31 (1983).
9. W.Coene and D.Van Dyck, Ultramicroscopy 15, 29.Ibid 15, 41; ibid 15, 287 (1984).
10. J.Van Landuyt, G.Van Tendeloo and S.Amelinckx, Crystal Growth and Characterization of Polytypes, p.343, Pergamon, (1983).
11. J.Van Landuyt, S.Amelinckx, J.A.Kohn and D.W.Eckart, J.Sol.St.Chem., 9, 103 (1974).
12. J.A.Wilson, F.J.Di Salvo and S.Mahajan, Phys.Rev.Lett.,32, 82 (1974).
13. P.M.Williams, G.S.Parry and C.B.Scruby, Phil.Mag., 29, 695 (1974).
14. J.Van Landuyt, G.Van Tendeloo and S.Amelinckx, Phys.Stat.Sol.(a), 26, 359 (1974).Ibid 26, 585 (1974); ibid 36, 767 (1976); ibid 42, 565 (1977).
15. C.F.Van Bruggen, C.Haas and G.A.Wiegers, J.Sol.St.Chem., 27, 9 (1979).
16. G.Van Tendeloo, J.Van Landuyt and S.Amelinckx, Phys.Stat.Sol.(a), 64, K105 (1981).
17. G.Van Tendeloo, J.Van Landuyt and S.Amelinckx, Phys.Stat.Sol.(a), 33, 723 (1976).
18. G.Dolino, J.P.Bachheimer, B.Berge, C.M.E.Zeyen, G.Van Tendeloo, J.Van Landuyt and S.Amelinckx, J.Phys.(Paris), 45, 901 (1984).

19.K.Gouhara and N.Kato, J.Phys.Soc.Jap., 53, 2177 (1984).
20.T.A.Aslanyan and A.P.Levanyuk, Sov.Phys.JETP Lett., 28, 70 (1978).
21.M.B.Walker, Phys.Rev.B., 28, 6407 (1983).
22.J.Van Landuyt, G.Van Tendeloo, S.Amelinckx and M.B. Walker, Phys.Rev.B, 31,(1985).